J Comput Electron (2016) 15:756–762
DOI 10.1007/s10825-016-0873-7

Manipulation of structural and optical behaviors in zincblende and wurtzite mercuric sulfide (HgS) nanocrystals: atomistic tight-binding theory

Worasak Sukkabot[1]

Published online: 27 July 2016

Abstract To obtain comprehensive information regarding the effect of size and geometric structure on the associated atomistic properties of mercuric sulfide (HgS) nanocrystals, the structural and optical properties of HgS semiconductor nanocrystals were explored numerically using atomistic tight-binding theory. The optical bandgap, charge density, density of states, electron–hole Coulomb energy, and optical spectrum were evaluated for different sizes and geometric structures. Size-dependent computations were realized by changing the diameter of the HgS nanocrystals. In addition, HgS nanocrystals with wurtzite and zincblende geometric structures were compared numerically. The theoretical results highlight that control of the electronic structure and optical properties of HgS nanocrystals can be achieved by changing their size and geometric structure. The dependence of the optical bandgap on the dimension of the HgS nanocrystals is mainly determined by quantum confinement. Finally, the optical properties of zincblende HgS nanocrystals are more promising than those of wurtzite HgS nanocrystals.

Keywords Tight-binding theory · HgS · Nanocrystals · Zincblende · Wurtzite

1 Introduction

Study of low-dimensional semiconductor structures is currently attracting great attention as an active field of research because their properties differ significantly from corresponding bulk materials. HgS is a II–VI semiconductor material. Because of its possible applications in acoustooptical materials [1], infrared sensing [2], and optoelectronic devices [3–5], mercuric sulfide (HgS) has been widely utilized. However, few reports are available on the nanostructure of HgS; For instance, Mahapatra and Dash [6] synthesized mercury sulfide (HgS) nanocrystals by a wet chemical route, obtaining nearly spherical HgS nanocrystals with average size of 9 nm. Xu et al. [7] reported a simple method to synthesize high-purity HgS nanoparticles without introducing surfactants or toxic chemicals. In addition, Onwudiwe and Ajibade [8] synthesized HgS nanoparticles by thermolysis of certain group 12 metal complexes as precursors. The obtained HgS nanoparticles clearly exhibited spherical shape. Ding and Zhu [9] introduced a novel route to prepare HgS nanocrystals in ethanol solvent in presence of sodium hydroxide using a microwave heating method. They found average dimension of approximately 10 and 6 nm. A systematic study on phase-transfer-based synthesis of HgS nanocrystals was reported by Han et al. [10], mainly presenting a pathway for producing HgS nanocrystals with desirable properties and analyzing the effect of their morphology. Although considerable experimental work has been carried out, theoretical reports on HgS nanocrystals are scarce. Therefore, in the present investigation, atomistic tight-binding theory was used to determine the atomistic behaviors, including the optical bandgap, charge density, density of states (DOS), electron–hole Coulomb energy, and optical spectrum, to provide comprehensive information regarding the effects of the dimension and geometric structure of HgS nanocrystals. The size of the HgS nanocrystals was varied by changing their diameter. Apart from the dimension, variation of the geometric structure, namely wurtzite or zincblende, is also a well-known approach to modify the natural properties of such materials.

✉ Worasak Sukkabot
w.sukkabot@gmail.com

[1] Department of Physics, Faculty of Science, Ubon Ratchathani University, 85 Sathollmark Rd. Warinchamrab, Ubon Ratchathani 34190, Thailand

To study the structural and optical properties of semiconductor nanocrystals, computational methods including the effective mass approximation (EMA) [11], atomistic empirical models [12–15], and first-principle calculations [16–18] have been implemented. The reason for using an atomistic model is to preserve an accurate and realistic description of the semiconductor nanocrystal material while retaining atomistic details and reducing computational requirements. For this reason, empirical tight-binding theory with sp^3s^* orbitals [19] and first nearest neighbor interaction was used in this study. Based on such detailed calculations based on atomistic tight-binding theory, the effects of the size and geometric structure on the natural behaviors of HgS nanocrystals can be clearly revealed.

This study investigates the atomistic effects of size and geometric structure on the structural and optical properties of HgS nanocrystals. The remainder of this paper is organized as follows: In Sect. 2, the computational steps are briefly described. The resulting calculations are discussed theoretically in Sect. 3. The main aim is to determine the impact of size and geometric structure on the atomistic properties of HgS nanocrystals based on the resulting data. Finally, a summary of the computations is presented in Sect. 4.

2 Theory and methodology

The computational process consisted of three steps. In the first step, the atomic positions for the wurtzite and zincblende structure were defined. The atomic positions of HgS nanocrystals were generated by cutting a spherical shape with desired diameter from bulk semiconductor without any surface relaxation effects, thus obtaining an unstrained nanocrystal [20]. To avoid gap states, dangling bonds on the surface of HgS nanocrystals were passivated using the technique described by Lee et al. [21]. In the second step, single-particle spectra were computed using atomistic tight-binding theory. This methodology has been effectively applied to study structural and optical properties of single and core–shell semiconductor nanocrystals [22–27]. The single-particle states are described as a linear combination of atomistic orbitals α situated on each atom R with N_{at} being the total number of atoms in the system, given by

$$\Psi = \sum_{R=1}^{N_{\text{at}}} \sum_{\alpha=1}^{5} C_{R,\alpha}\varphi_{\alpha}(\vec{r} - \vec{R}).$$

The empirical tight-binding Hamiltonian [28] was modified to include the spin–orbit interaction, being given by

Table 1 Calculated bandgap of bulk zincblende HgS semiconductor

Method	Bandgap (eV)
Atomistic tight-binding theory	0.20
QSGW [31]	0.61
h-QSGW [31]	0.37
Corrected local density approximation method [32]	0.30

$$H_{\text{TB}} = \sum_{R=1}^{N_{\text{at}}} \sum_{\alpha=1}^{5} \varepsilon_{R\alpha} \mathrm{c}^{\dagger}_{R\alpha} \mathrm{c}_{R\alpha} + \sum_{R=1}^{N_{\text{at}}} \sum_{R'=1}^{N_{\text{at}}} \sum_{\alpha=1}^{5} \sum_{\alpha'=1}^{5} t_{R\alpha,R'\alpha'} \mathrm{c}^{\dagger}_{R\alpha} \mathrm{c}_{R'\alpha'}.$$

The operator $\mathrm{c}^{\dagger}_{R\alpha}$ ($\mathrm{c}_{R\alpha}$) creates (annihilates) a particle in orbital α of atom R. In this work, the sp^3s^* tight-binding model [19] with first nearest neighbor interaction was utilized for the computation. Using the parameterization from [29], the on-site orbital energies $\varepsilon_{R\alpha}$ and the hopping matrix elements $t_{R\alpha,R'\alpha'}$ were obtained numerically using the Slater–Koster rules [30]. The single-particle energies and states were obtained computationally by diagonalizing the matrix of the empirical tight-binding Hamiltonian. In addition, we present a detailed comparison among the atomistic tight-binding theory, the quasiparticle self-consistent GW (QSGW) approximation [31], the hybrid QSGW scheme (h-QSGW) [31], and the corrected local density approximation method [32]. The bandgap calculated for bulk zincblende HgS semiconductor is also listed in Table 1. The results of these computations underline that the bandgaps calculated based on tight-binding theory are mainly consistent with those obtained using the h-QSGW and corrected local density approximation methods. After obtaining the single-particle spectra for wurtzite and zincblende HgS nanocrystals of several diameters, the exciton and optical properties were investigated in the third step. The excitonic states and energies were obtained by including the tight-binding single-particle states and energies in the excitonic Hamiltonian. The Hamiltonian of single excitonic states is defined as

$$H = \sum_{i} E_i \mathrm{e}^{\dagger}_i \mathrm{e}_i + \sum_{j} E_j \mathrm{h}^{\dagger}_j \mathrm{h}_j - \sum_{ijkl} V^{\text{eh}}_{ijkl} \mathrm{h}^{\dagger}_i \mathrm{e}^{\dagger}_j \mathrm{e}_k \mathrm{h}_l.$$

The first two terms here are the electron and hole single-particle energies, respectively, while the last term describes the electron–hole Coulomb interaction. The equation for the excitonic states (Φ_{ex}) is $\sum_{i,j} B_{i,j} \Psi^{\text{e}}_i(r) \Psi^{\text{h}}_j(r)$, with $\Psi^{\text{e}}_i(r)$ and $\Psi^{\text{h}}_j(r)$ being the ith electron and jth hole single-particle states, respectively. To analyze the optical properties of HgS nanocrystals with different structures and diameters, the optical spectra between electron and hole levels were defined as

Table 2 Number of atoms in wurtzite (WZ) and zincblende (ZB) HgS nanocrystals as function of diameter (D_c)

Diameter (D_c) (nm)	Wurtzite (WZ)	Zincblende (ZB)
2.00	165	159
2.50	325	329
3.00	570	597
3.50	886	885
4.00	1340	1339
4.50	1876	1911
5.00	2607	2593

$$I(E) = \frac{2\pi}{\hbar} \sum_{e,h} \left| \hat{e} \cdot \vec{D}_{e,h} \right|^2 \delta (E_e - E_h - E).$$

Here, $\delta (E_e - E_h - E) = \frac{1}{\sigma\sqrt{2\pi}} e^{(-\frac{(E_e - E_h - E)^2}{2\sigma^2})}$ with $\sigma = 1.0$ meV being the spectral line broadening. E_e and E_h are the single-particle energies of electron and hole states, respectively. $\vec{e}$ are the polarized vectors. $\vec{D}_{e,h}$ are the dipole moments for interband transitions of electron and hole states.

3 Results and discussion

To determine the effects of the size and geometric structure on the structural and optical properties of HgS nanocrystals, an sp^3s^* empirical tight-binding description was numerically utilized for HgS nanocrystals with zincblende (ZB) or wurtzite (WZ) crystal structure and spherical shape. The atom located at the center of the nanocrystal was an anion. HgS nanocrystals with diameter (D_c) of 2.00, 2.50, 3.00, 3.50, 4.00, 4.50, and 5.00 nm were employed as the structural candidates in the simulations. The number of atoms in the HgS nanocrystals with different diameters and geometric structures is summarized in Table 2, clearly showing that the number of atoms in the HgS nanocrystal increased with increasing diameter. Meanwhile, the geometric structure did not affect the tendency in the number of atoms.

We start with the dependence of the bandgap on the size and geometric structure of the HgS nanocrystal; the calculations with various diameters and geometric structures are illustrated in Fig. 1. The energy difference between the ground single-electron and single-hole states is defined as the single-particle gap. The excitonic energies were obtained numerically using the configuration interaction (CI) description. The number of conduction and valence states required to achieve the desired convergence was typically 12 each. As can be expected based on the quantum confinement hypothesis, the optical bandgap was mainly sensitive to the total number of atoms in the nanocrystal. The results show that the

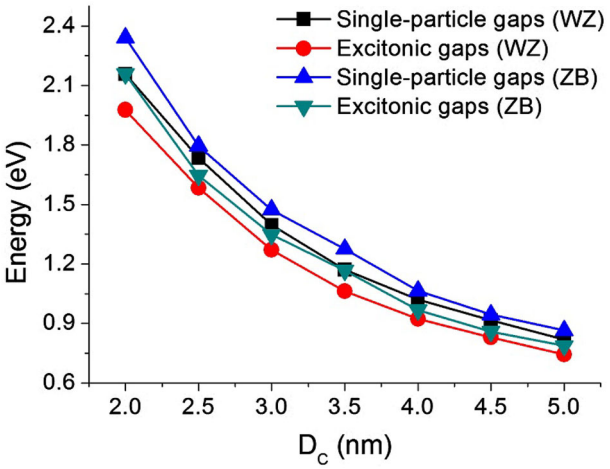

Fig. 1 Optical bandgap of wurtzite (WZ) and zincblende (ZB) HgS nanocrystals as function of diameter (D_C)

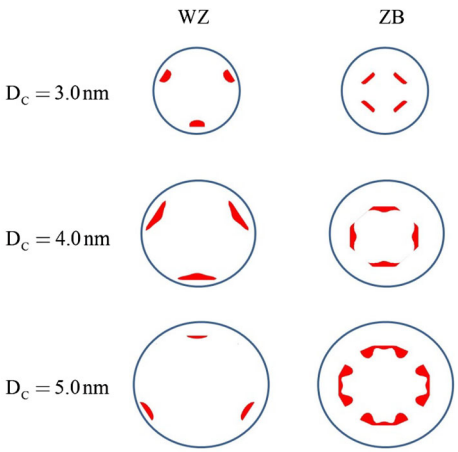

Fig. 2 First electron charge density of three selected wurtzite (WZ) and zincblende (ZB) HgS nanocrystals

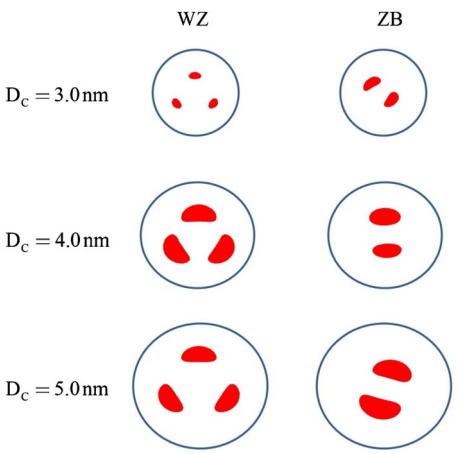

Fig. 3 First hole charge density of three selected wurtzite (WZ) and zincblende (ZB) HgS nanocrystals

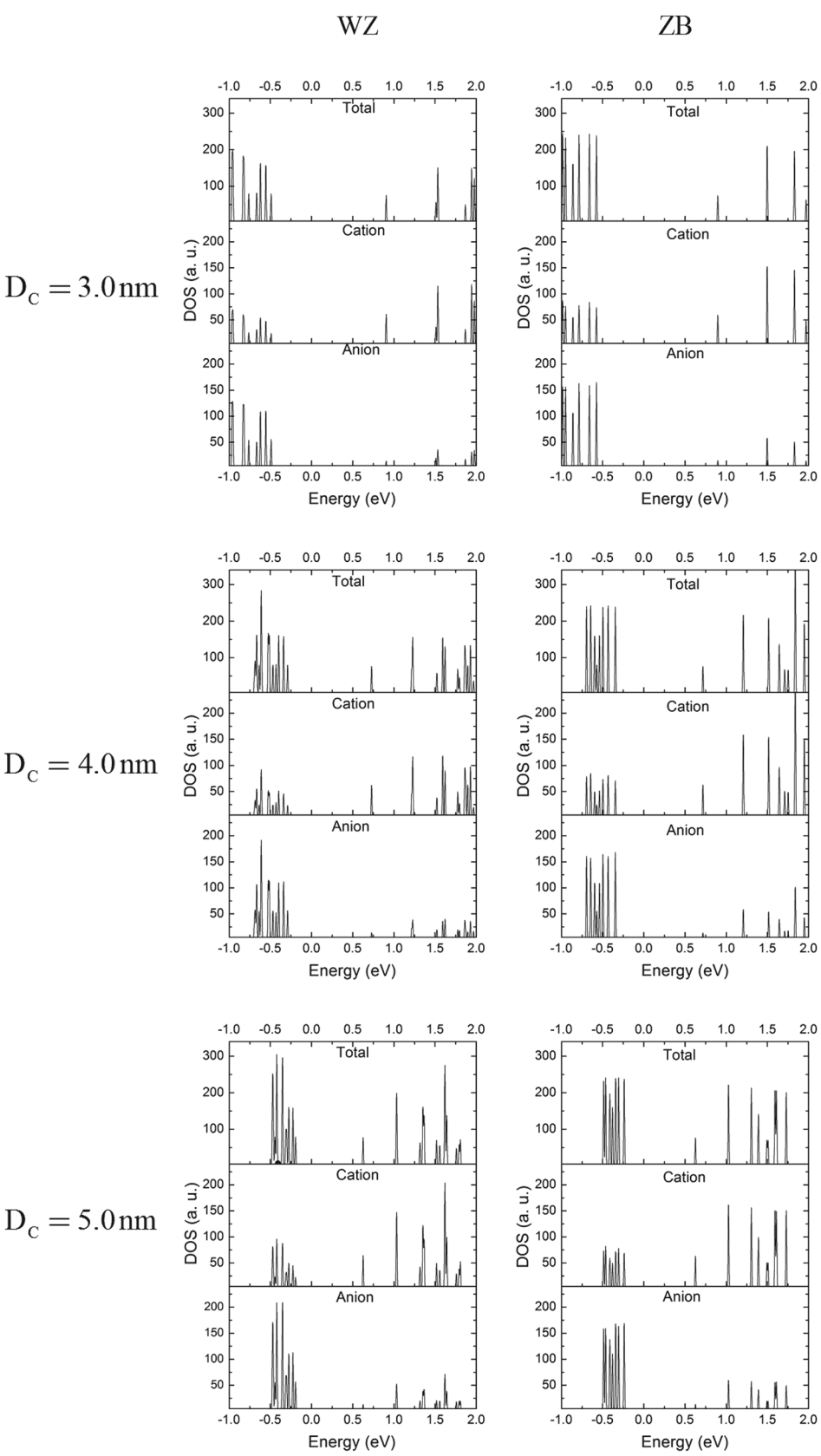

Fig. 4 Density of states (DOS) of three selected wurtzite (WZ) and zincblende (ZB) HgS nanocrystals

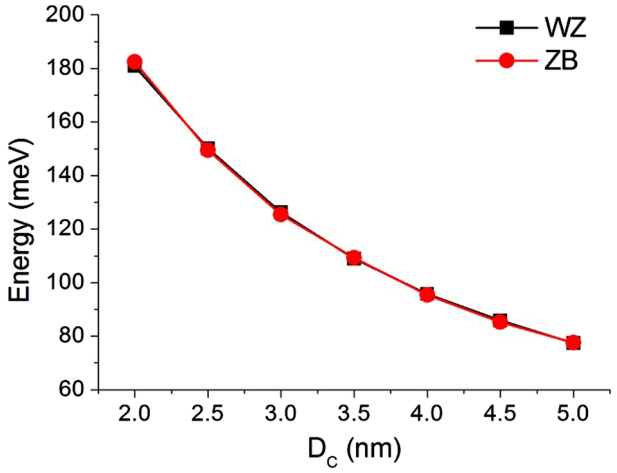

Fig. 5 Ground electron–hole Coulomb energy of wurtzite (WZ) and zincblende (ZB) HgS nanocrystals as function of diameter (D_C)

reduction in the bandgap with increasing diameter generally corresponds to the increase in the number of atoms. Interestingly, the optical bandgap of zincblende HgS nanocrystals is greater than for wurtzite structure. This can be explained based on the dependence of the optical bandgap on the structural phase transition. The optical bandgap is improved for the zincblende rather than wurtzite structure. As a result, the optical bandgap of the HgS nanocrystals can be appropriately controlled by changing their dimension and geometric structure to identify promising candidates for use in optoelectronic applications. In addition, the charge density of ground electron and hole states in wurtzite and zincblende HgS nanocrystals is displayed in Figs. 2 and 3, respectively. The dependence of the electron and hole charge density on the dimension and geometric structure is clearly observed. In terms of the ground electron state, the electron is localized near the surface of the HgS nanocrystal. With increasing diameter, the electron charge density spreads widely outward to the surface. The electron charge density is more confined close to the central region in the zincblende compared with the wurtzite HgS nanocrystals. In terms of the ground hole state, the hole is mostly localized around the center in the zincblende and wurtzite HgS nanocrystals. Akin to the electron states, the hole charge density expands as the diameter is increased.

The density of states (DOS) for three selected wurtzite and zincblende HgS nanocrystals is plotted in Fig. 4. The partial density of states (PDOS) for the contribution of anion and cation atoms is also shown. The amplitudes and pattern of the density of states (DOS) for the HgS nanocrystals are essentially dependent on the diameter and geometric structure. As the diameter increases, the conduction- and valence-band edges decrease and increase, respectively. These results also reveal that the main contribution to the conduction and valence bands for both wurtzite and zincblende HgS nanocrystals is due to cations and anions, respectively. In terms of the geometric structure, the amplitude of the density of states (DOS) for the zincblende HgS nanocrystals is more pronounced than for the wurtzite HgS nanocrystals.

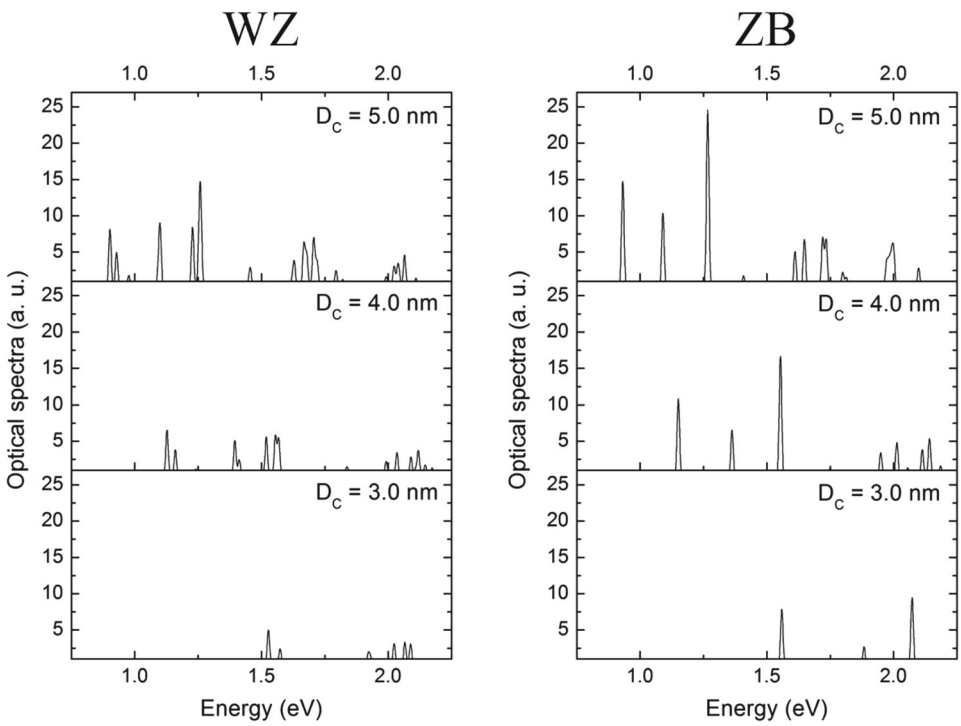

Fig. 6 Optical spectra of three selected wurtzite (WZ) and zincblende (ZB) HgS nanocrystals

The electron and hole confinement in the HgS nanocrystals was analyzed as a function of their size and geometric structure based on the electron–hole Coulomb interaction. The ground-state Coulomb energy of the wurtzite and zincblende HgS nanocrystals as a function of diameter is presented in Fig. 5. With increasing diameter, reduction in the Coulomb energy is clearly observed. As a result, weak electron and hole confinement is demonstrated with increasing dimension. Nevertheless, the electron–hole Coulomb interaction is not affected by the geometric structure of the HgS nanocrystals.

Finally, the optical spectra of three selected wurtzite and zincblende HgS nanocrystals are presented in Fig. 6. The optical spectra clearly depend on the dimension and geometric structure. As the size of the HgS nanocrystal was increased, red-shift of the optical spectrum was obviously demonstrated. The optical intensity was enhanced with increasing diameter. Regarding the geometric structure, the intensity of the optical spectra for zincblende HgS nanocrystals was much greater than for the wurtzite HgS nanocrystals. It is expected that the optical properties of zincblende HgS nanocrystals will be better compared with wurtzite HgS nanocrystals. Such knowledge regarding control of the optical properties by variation of the dimension and geometric structure could be used to identify materials with parameter values suitable for use in optical applications.

4 Conclusions

The size-dependent structural and optical properties of wurtzite and zincblende HgS nanocrystals were determined using sp^3s^* empirical tight-binding (TB) theory. The results of the atomistic computations prominently depend on the size and geometric structure of the HgS nanocrystals. The quantum confinement effect is indicated by a reduction in the optical bandgap. As observed from the density of states (DOS), the contributions to the conduction and valence bands in HgS nanocrystals are primarily due to cation and anion atoms, respectively. The atomistic electron–hole Coulomb interaction indicates that electrons and holes are weakly confined in bulk-sized HgS nanocrystals, but with no dependence on the geometric structure. In addition, enhancement of the optical properties is found for zincblende HgS nanocrystals. Finally, manipulation of the structural and optical properties of HgS nanocrystals by variation of their dimension and geometric structure can offer dynamic guidelines for selection of materials with parameters suitable for use in nanodevices based on this material.

Acknowledgments This work has been kindly supported by Department of Physics, Faculty of Science, Ubon Ratchathani University.

References

1. Sapriel, J.: Cinnabar (α HgS), a promising acousto-optical material. Appl. Phys. Lett. **19**, 533–535 (1971)
2. Higginson, K.A., Kuno, M., Bonevich, J., Qadri, S.B., Yousuf, M., Mattoussi, H.: Synthesis and characterization of colloidal β-HgS quantum dots. J. Phys. Chem. B **106**, 9982–9985 (2002)
3. Chakraborty, I., Mitra, D., Moulik, S.P.: Spectroscopic studies on nanodispersions of CdS, HgS, their core–shells and composites prepared in micellar medium. J. Nanopart. Res. **7**, 227–236 (2005)
4. Kershaw, S.V., Harrison, M., Rogach, A.L., Kornowski, A.: Development of IR-emitting colloidal II–VI quantum-dot materials. IEEE J. Sel. Top. Quantum Electron. **6**, 534–543 (2000)
5. Roberts, G.G., Lind, E.L., Davis, E.A.: Photoelectronic properties of synthetic mercury sulphide crystals. J. Phys. Chem. Solids **30**, 833–844 (1969)
6. Mahapatra, A.K., Dash, A.K.: α-HgS nanocrystals: synthesis, structure and optical properties. Phys. E **35**, 9–15 (2006)
7. Xin, Xu, Carraway, E.R.: Sonication-assisted synthesis of β-mercuric sulfide nanoparticles. Nanomater. Nanotechnol. **2**, 17–22 (2012)
8. Onwudiwe, D.C., Ajibade, A.: ZnS, CdS and HgS nanoparticles via alkyl-phenyl dithiocarbamate complexes as single source precursors. Int. J. Mol. Sci. **12**, 5538–5551 (2011)
9. Ding, T., Zhu, J.-J.: Microwave heating synthesis of HgS and PbS nanocrystals in ethanol solvent. Mater. Sci. Eng. B **100**, 307–313 (2003)
10. Han, L., Hou, P., Feng, Y., Liu, H., Li, J., Peng, Z., Yang, J.: Phase transfer-based synthesis of HgS nanocrystals. Dalton Trans. **43**, 11981–11987 (2014)
11. Hemdana, I., Mahdouani, M., Bourguiga, R.: Investigation of the radiative lifetime in core–shell CdSe/ZnS and CdSe/ZnSe quantum dots. Phys. B **407**, 3313–3319 (2012)
12. Williamson, A.J., Zunger, A.: Pseudopotential study of electron–hole excitations in colloidal free-standing InAs quantum dots. Phys. Rev. B **61**, 1978–1991 (2000)
13. Wang, L.W., Zunger, A.: Electronic structure pseudopotential calculations of large (approx. 1000 atoms) Si quantum dots. J. Phys. Chem. **98**, 2158–2165 (1994)
14. Leung, K., Whaley, K.B.: Electron–hole interactions in silicon nanocrystals. Phys. Rev. B **56**, 7455–7468 (1997)
15. Niquet, Y.M., Delerue, C., Lannoo, M., Allan, G.: Single-particle tunneling in semiconductor quantum dots. Phys. Rev. B **64**, 113305–113308 (2001)
16. Luo, Y., Wang, L.-W.: Electronic structures of the CdSe/CdS core–shell nanorods. ACS Nano **4**(1), 91–98 (2010)
17. Yang, S., Prendergast, D., Neaton, J.B.: Strain-induced band gap modification in coherent core/shell nanostructures. Nano Lett. **10**(8), 3156–3162 (2010)
18. Khoo, K.H., Arantes, J.T., Chelikowsky, J.R., Dalpian, G.M.: First-principles calculations of lattice-strained core–shell nanocrystals. Phys. Rev. B **84**, 075311–075317 (2011)
19. Vogl, P., Hjalmarson, H.P., Dow, J.D.: A Semi-empirical tight-binding theory of the electronic structure of semiconductors. J. Phys. Chem. Solids **44**, 365–378 (1983)
20. Alivisatos, A.P.: Semiconductor clusters, nanocrystals, and quantum dots. Science **271**, 933–937 (1996)
21. Lee, S., Oyafuso, F., von Allmen, P., Klimeck, G.: Boundary conditions for the electronic structure of finite-extent embedded semiconductor nanostructures. Phys. Rev. B **69**, 045316–045323 (2004)
22. Sukkabot, W.: Electronic structure and optical properties of colloidal InAs/InP core/shell nanocrystals: tight-binding calculations. Phys. E Low Dimens. Syst. Nanostruct. **63**, 235–240 (2014)

23. Sukkabot, W.: Influence of ZnSe core on the structural and optical properties of ZnSe/ZnS core/shell nanocrystals: tight-binding theory. Superlattices Microstruct. **75**, 739–748 (2014)
24. Sukkabot, W.: Tight-binding theory of the excitonic states in colloidal InSb nanostructures. Mater. Sci. Semicond. Process. **27**, 51–55 (2014)
25. Sukkabot, W.: Atomistic tight-binding theory in CdSe/ZnSe wurtzite core/shell nanocrystals. Comput. Mater. Sci. **96**, 336–341 (2014)
26. Sukkabot, W.: Role of structural and compositional details in atomistic tight-binding calculations for InN nanocrystals. Mater. Sci. Semicond. Process. **38**, 142–148 (2015)
27. Sukkabot, W.: Structural properties of SiC zinc-blende and wurtzite nanostructures: atomistic tight-binding theory. Mater. Sci. Semicond. Process. **40**, 117–122 (2015)
28. Korkusinski, M., Voznyy, O., Hawrylak, P.: Fine structure and size dependence of exciton and biexciton optical spectra in CdSe nanocrystals. Phys. Rev. B **82**, 245304–245319 (2010)
29. Bryant, G.W., Jaskólski, W.: Tight-binding theory of quantum-dot quantum wells: single-particle effects and near-band-edge structure. Phys. Rev. B **67**, 205320–205336 (2003)
30. Slater, J.C., Koster, G.F.: Simplified LCAO method for the periodic potential problem. Phys. Rev. **94**, 1498–1524 (1954)
31. Svane, A., Christensen, N.E., Cardona, M., Chantis, A.N., van Schilfgaarde, M., Kotani, T.: Quasiparticle band structures of β-HgS, HgSe, and HgTe. Phys. Rev. B **84**, 205205–205210 (2011)
32. Moon, C.-Y., Wei, S.-H.: Band gap of Hg chalcogenides: symmetry-reduction-induced band-gap opening of materials with inverted band structures. Phys. Rev. B **74**, 045205–045209 (2006)